

A study of the structural controls on oil recovery from shallow-marine reservoirs

T. Manzocchi¹, J. D. Matthews², J. A. Strand^{1,6}, J. N. Carter², A. Skorstad³, J. A. Howell⁴,
K. D. Stephen⁵ and J. J. Walsh¹

¹*Fault Analysis Group, UCD School of Geological Sciences, University College Dublin, Dublin 4, Ireland
(e-mail: tom@fag.ucd.ie)*

²*Department of Earth Science and Engineering, Imperial College, London SW7 2BP, UK*

³*Norwegian Computing Center, PO Box 114 Blindern, N-0314 Oslo, Norway*

⁴*Department of Earth Science/Centre for Integrated Petroleum Research, University of Bergen, Allengt. N-5007 Bergen, Norway*

⁵*Institute of Petroleum Engineering, Heriot-Watt University, Edinburgh EH9 9NX, UK*

⁶*Current address: CSIRO Petroleum, PO Box 1130, Bentley, WA6102, Australia*

ABSTRACT: The differences in oil production are examined for a simulated waterflood of faulted and unfaulted versions of synthetic shallow-marine reservoir models with a range of structural and sedimentological characteristics. Fault juxtaposition can reduce the economic value of the reservoirs by up to 30%, with the greatest losses observed in models with lower sedimentological aggradation angles and faults striking parallel to waterflood direction. Fault rock has a greater effect than fault juxtaposition on lowering the economic value of the reservoir models in the compartmentalized cases only – and only when the fault rock permeability model is based on the least permeable published laboratory data. Moderately sealing faults can increase the economic value of reservoirs except when the main flow direction is parallel to the faults. These results arise from the dependence of economic value on both sweep efficiency and production rate. Simple predictors of fault juxtaposition and fault-rock heterogeneity have been established and combined with two-dimensional considerations from streamline theory in an attempt to capture quantitatively the change in economic reservoir value arising from faults. Despite limitations associated with the three-dimensional role of juxtaposition, the results are encouraging and represent a step towards establishing a rapid transportable predictor of the effects of faults on production.

KEYWORDS: *oil production, shallow marine, faults, transmissibility multipliers, uncertainty, sensitivity*

INTRODUCTION

This paper examines systematically the differences in performance between faulted and unfaulted versions of synthetic shallow-marine reservoir models. The objective of the work is to understand these differences as a function of geological characteristics of the models and, based on this understanding, to attempt to define a generic and transportable method for predicting the effects of faults using sedimentological and structural characteristics that might be known or could be estimated during a field appraisal. Previous studies addressing purely sedimentological aspects have indicated that measures of the geometrical distribution of permeability (particularly its connectivity and anisotropy) discriminate reservoir performance better than conventional geological characteristics (e.g. Jian *et al.* 2004; Larue & Legarre 2004); this paper applies similar considerations to assess the effects of faults.

An overview of the larger modelling programme (the 'SAIGUP' study) from which the presented work derives is given by Manzocchi *et al.* (2008a). In the present paper a detailed quantitative description of the various fault models

used in the study is presented, before the effects of faults on production are described using full-field simulation results of *c.* 18 000 model reservoirs. Two parameters measured in the static models are found to provide unbiased calibrations with the effects of the faults on an economic measure of reservoir value, and methods for estimating these parameters from basic sedimentological and structural characteristics are addressed in the fourth section. In the subsequent section, two-dimensional conceptualizations from streamline theory are combined with an empirical predictor of the fractional permeability of 2D faulted areas, in an attempt to define a general predictor of the change in reservoir value as a function of the different geometrical and petrophysical characteristics of the fault systems.

This paper concentrates exclusively on models in which faults are represented as planar surfaces between grid-blocks, with the fault-rock properties (fault permeability and thickness) included as transmissibility multipliers and modelled as deterministic functions of fault surface shale gouge ratio and throw respectively. Reservoir models which include stochastic variability of fault-rock permeability and which depart from the conventional assumption in flow simulation of planar fault

surfaces and single-phase fault-rock properties to include the fully 3D flow geometries associated with fault relay zones as well as two-phase fault-rock properties, are examined elsewhere (Manzocchi *et al.* 2008b).

STRUCTURAL DETAILS OF THE SIMULATION MODELS

The synthetic reservoir models used in the SAIGUP study have been built as a function of four separate sets of parameter variables, each of which is a function of several others (Manzocchi *et al.* 2008a). These primary sets of variables are: (i) the reservoir sedimentology (reviewed briefly below and described in detail by Howell *et al.* 2008); (ii) the reservoir structure (described below); (iii) the well configurations and controls (described by Matthews *et al.* 2008); and (iv) the upscaling method used to generate the simulation model grid-block pseudoproperties (described by Stephen *et al.* 2008). The focus here is principally on the effects of interactions between sedimentological and structural model characteristics, but the effects of the different well configurations are also addressed to some extent. Effects of upscaling are not discussed and all simulation results used here derive from models with the same set of six facies-specific upscaled cell pseudoproperties (see Matthews *et al.* 2008 for details).

Sedimentologically, the 9 km × 3 km × 80 m models are characterized by five variables (Howell *et al.* 2008; Manzocchi *et al.* 2008a). The progradation direction defines the absolute dip-direction of the facies, either parallel to the strike direction of the reservoir, towards the structural high or away from the structural high. The number of zones (parasequences) in each model is also a discrete setting, with the majority of the models having four 20 m thick parasequences, but a few have been built with two or six parasequences. The percentage coverage of the parasequence-bounding, and clinoform surface, cements are fixed at three levels (10%, 50%, 90%) but the locations of clinoforms and locations of holes in the cemented surfaces are defined stochastically. The aggradation angles of the model facies are defined as low, medium or high for an entire model, and the values defining the absolute aggradation angles in each parasequence are drawn from uniform distributions around a mean value (0.2°, 0.65° or 1.2°). Similarly, the curvature of the shoreline is defined by a value drawn from a distribution to model the shorelines in each parasequence. The models range from parallel, wave-dominated shorelines (low curvature) to river-dominated systems (high curvature). Other variables for each model or parasequence are also drawn independently from predefined distributions (e.g. the location of the shoreline in the lowermost parasequence and factors defining the horizontal offset of facies across parasequence boundaries; see Howell *et al.* (2008) for further details), and the precise combination of variables in any particular model defines the basic sedimentological architecture.

Gross reservoir structure

All the models share a basic template of an uplifted footwall trap controlled by structural closure and have the same oil-water contact and gross-rock volume (Fig. 1). The formation dip perpendicular to the long axis of the reservoirs is $\approx 7.3^\circ$, representative of many Viking Graben reservoirs (Table 1). Four end-member structure models are used, constructed deterministically from natural examples (Fig. 1). These are:

- structure A – a predominantly strike-parallel fault system (Fig. 1a) based on the fault system in the Beatrice Field in the Inner Moray Firth, offshore UK (e.g. Stevens 1991);

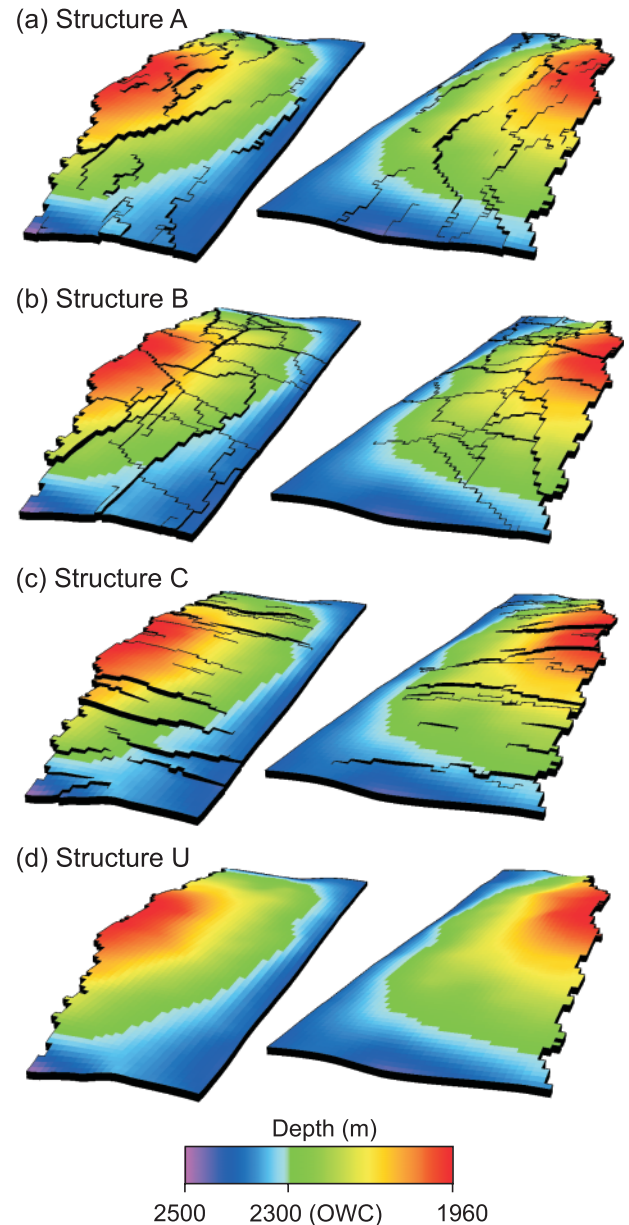


Fig. 1. Views of the four end-member reservoir structures: (a) structure A; (b) structure B; (c) structure C; (d) structure U. Structures A, B and C are shown at their maximum fault density levels (i.e. A1, B1 and C1). The models are 9 km × 3 km × 80 m.

- structure B – a more isotropic, compartmentalized fault system comprising approximately equal densities of strike-parallel and strike-perpendicular faults (Fig. 1b) based on a portion of the Gullfaks Field (e.g. Yielding *et al.* 1999);
- structure C – a strike-perpendicular fault system based on faults from an area adjacent to Lake Bogoria in the East African Rift (Fig. 1c);
- structure U – an unfaulted reservoir model with the same overall form as the three faulted structures (Fig. 1d).

Each of the three faulted structures are sampled at three different levels of strain to define the nine faulted models used throughout. The (dimensionless) strain measure (γ) used is the sum of the geometric moments (Scholz & Cowie 1990) of all faults in the system, normalized by the reservoir area (A). This is:

Table 1. Top reservoir and formation dips for selected North Sea reservoirs

Field	Formation	Locality	Top structure dip (°)	Formation dip (°)	Source
Gullfaks	Cook	Viking Graben	0.6	9	Yielding <i>et al.</i> (1999)
Brent	Statfjord	Viking Graben	3.2	8	James <i>et al.</i> (1999)
Fulmar	Fulmar	Viking Graben	4	12.5	Spaak <i>et al.</i> (1999)
Heron	Skagerrak	Central North Sea	13.1	16.9	Pooler & Amory (1999)
Shearwater	Fulmar	Central North Sea	14.5	18.4	Blehaut <i>et al.</i> (1999)
Beatrice	Various	Inner Moray Firth	6	6	Stevens (1991)

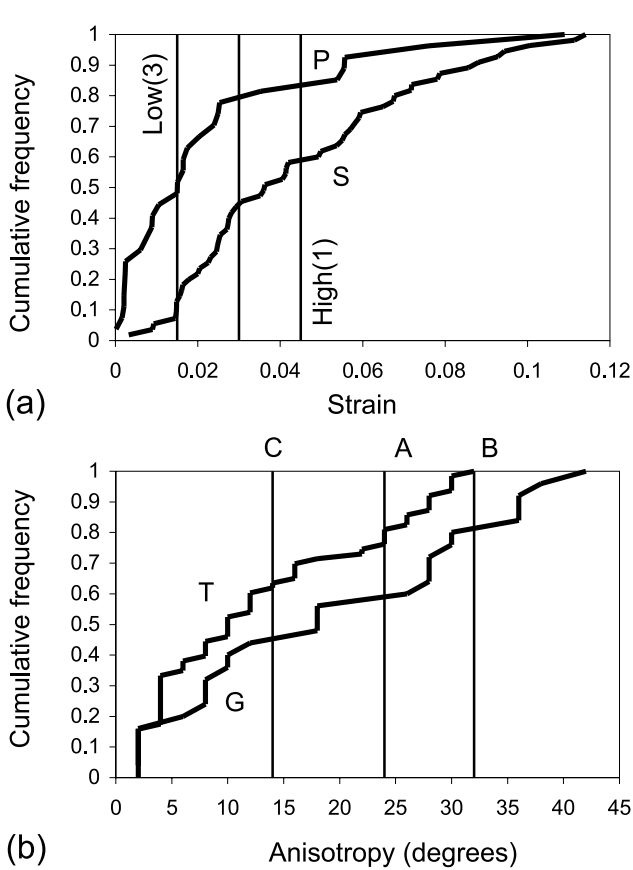


Fig. 2. Parameters of normal fault systems measured from seismic interpretation. (a) Strain level (P: 27 post-depositional fault systems. S: 55 syn-depositional fault systems). (b) Fault orientation anisotropy (°), see text for definition. (T: 64 tectonic fault systems. G: 26 gravity-driven fault systems). The vertical lines mark the positions of the modelled reservoirs (strain code 3 is low fault density, while code 1 is high density).

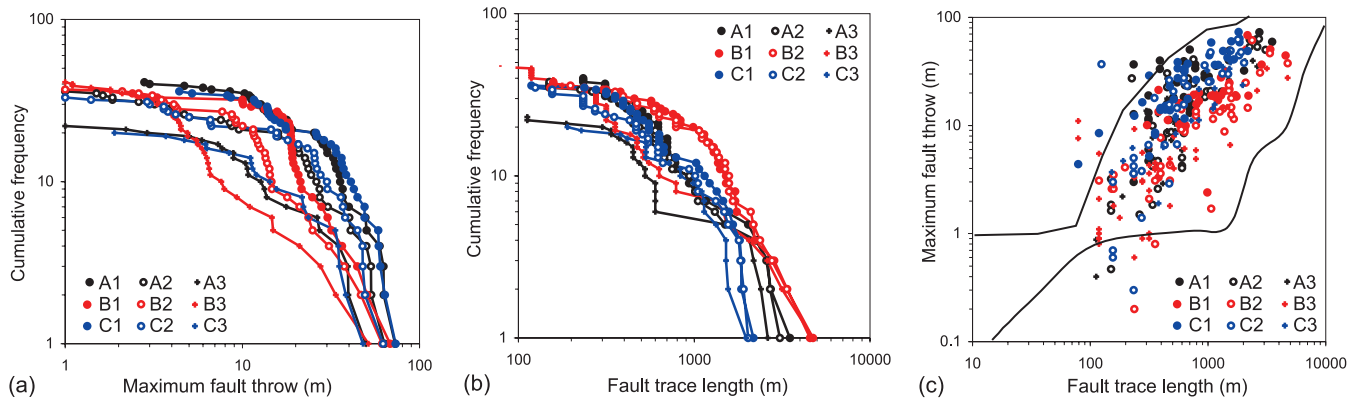


Fig. 3. (a) Maximum fault throw populations, (b) fault length populations and (c) fault trace length vs. maximum throw for the nine models. The outlined area on (c) indicates the region containing measurements of natural faults (Schlishe *et al.* 1996).

$$s = \frac{1}{A} \sum_{i=1}^N \int_0^L t dL \quad (1)$$

where N is the total number of faults in the system, and t is the local throw along the total length (L) of the individual faults. The strain levels used are 0.045, 0.03 and 0.015, values which are representative of natural post-depositional fault systems (Fig. 2a). The high strain versions of the three structures are referred to in this study as structures A1, B1 and C1 (shown in Fig. 1), the medium-strain versions as A2, B2 and C2, and the low-strain versions as A3, B3 and C3. Both the trace lengths and throw profiles of larger faults differ with different strain levels, and the smaller faults in the high strain versions are absent from the lower strain versions (see Manzocchi *et al.* 2008a, fig. 5). Figure 3 shows the maximum throw and fault trace length populations for the nine models. Structures A and C share very similar fault populations at equivalent strain levels, while structure B contains longer but lower throw faults. Figure 3c indicates that the faults in structures A and C have horizontal throw gradients (i.e. t_{\max}/L ratios) towards the upper end of ranges recorded for natural faults, while those in structure B lie closer to the centre of the range covered by the natural data.

Summary statistics of the fault systems are reported in Table 2. The anisotropy of a fault system is parameterized as an angle separating two fault orientations (α) such that, if all the faults were divided equally between these orientation populations, the scan-line density (i.e. frequency of faults per metre) recorded in any direction is the same as in the fault system (Manzocchi 2002). If $\alpha=45^\circ$ the fault system is isotropic and, in Table 2, lower and higher values indicate faults striking preferentially perpendicular and parallel to the waterflood direction, respectively. The values calculated for the three structures (Table 2) are within the ranges measured in natural tectonic fault systems (Fig. 2b).

Table 2. Summary statistics of the nine faulted structures

Structure	Strain	Number of faults	Maximum throw (m)	Anisotropy (α)	Fault length/area (m/m^2)	Discretized length/area (m/m^2)	Areal fraction of faulted connections	Line density (d_L)	Mean \log_{10} (length, m)	Standard deviation \log_{10} (length, m)	Critical line density (d_{LC})	Proximity to connectivity threshold (D)
A1	0.045	41	72.8	24	0.00151	0.00251	0.0756	0.559	2.803	0.31	1.05	0.47
A2	0.03	36	63.35	24	0.00134	0.00219	0.0638	0.477	2.775	0.34	1.05	0.55
A3	0.015	23	49.7	24	0.000823	0.00115	0.0413	0.305	2.736	0.38	1.05	0.71
B1	0.045	35	68.3	34	0.00199	0.0026	0.0952	0.931	3	0.31	0.9	-0.03
B2	0.03	38	61.4	34	0.00199	0.00252	0.0916	0.954	2.9	0.39	0.9	-0.06
B3	0.015	49	51.4	34	0.00134	0.00179	0.0625	0.613	2.663	0.42	0.9	0.32
C1	0.045	36	73.2	76	0.00133	0.00172	0.0612	0.387	2.79	0.33	1.7	0.77
C2	0.03	35	62.3	76	0.00113	0.00151	0.0535	0.32	2.716	0.35	1.7	0.81
C3	0.015	20	47.9	76	0.00082	0.00109	0.0392	0.23	2.845	0.31	1.7	0.86

Line density (d_L) is a (dimensionless) function of fault length and reservoir area, defined as:

$$d_L = \frac{\sum_{i=1}^N L^2}{4A}. \quad (2)$$

Combined with the anisotropy of the fault system, d_L is an important measure of fault connectivity (e.g. Robinson 1983; Bour & Davy 1997) and therefore, in the case of low permeability faults, of reservoir compartmentalization. Although fault systems are generally perceived to follow power-law distributions, a scale-bound sample in a finite area is often better described by a log-normal distribution (e.g. Bonnet *et al.* 2001), and Table 2 records the mean and standard deviation of the best fit log-normal distribution of the fault length populations. A representative fault system becomes compartmentalized at its critical line density (d_{LC}), and the d_{LC} values reported in Table 2 have been calculated as a function of the ratio of fault abutments to intersections, the best-fit log normal fault length distributions and the fault system anisotropy values, using the model of Manzocchi (2002). The term D , given by $D=1-d_L/d_{LC}$, represents the proximity of the fault system to its connectivity threshold and, like s and a , will be used later to estimate the effects of the different fault systems on reservoir production.

In order that the sedimentological models can all be constructed using the same grid-block sizes, the model faults have been aliased to the edges of square grid-blocks (Fig. 1). The effect of this discretization can be observed by comparing the values of the discretized and undiscretized fault trace length/area, which show an increase of between 20% and 40% in the fault length present as a function of discretization (Table 2). Faulted connections occupy between 3.9% and 9.5% by area of all active connections in the faulted models.

Fault-rock properties

Fault-rock permeability is modelled deterministically as a function of shale gouge ratio (SGR; Yielding *et al.* 1997) and fault-rock thickness as a function of fault throw. Fault-rock permeability and thickness are then combined with other model properties to define transmissibility multipliers for each faulted connection using the TransGen fault property modelling software (e.g. Manzocchi *et al.* 1999; Childs *et al.* 2002; Yielding 2002). Eight fault permeability cases are considered, ranging from relatively sealing to relatively transmissible, and covering the ranges of previously proposed relationships (e.g. Manzocchi *et al.* 1999; Crawford *et al.* 2002; Sperrevik *et al.* 2002). These

cases (shown in Fig. 4a) are given by the relationships (K_f is fault permeability in mD; SGR is a fraction):

$$\begin{aligned} \text{Case 1: } K_f &= 10^{0.4-4SGR} \\ \text{Case 2: } K_f &= 10^{-0.6-4SGR} \\ \text{Case 3: } K_f &= 10^{-1.4-3.2SGR} \\ \text{Case 4: } K_f &= 10^{-1.6-4SGR} \end{aligned}$$

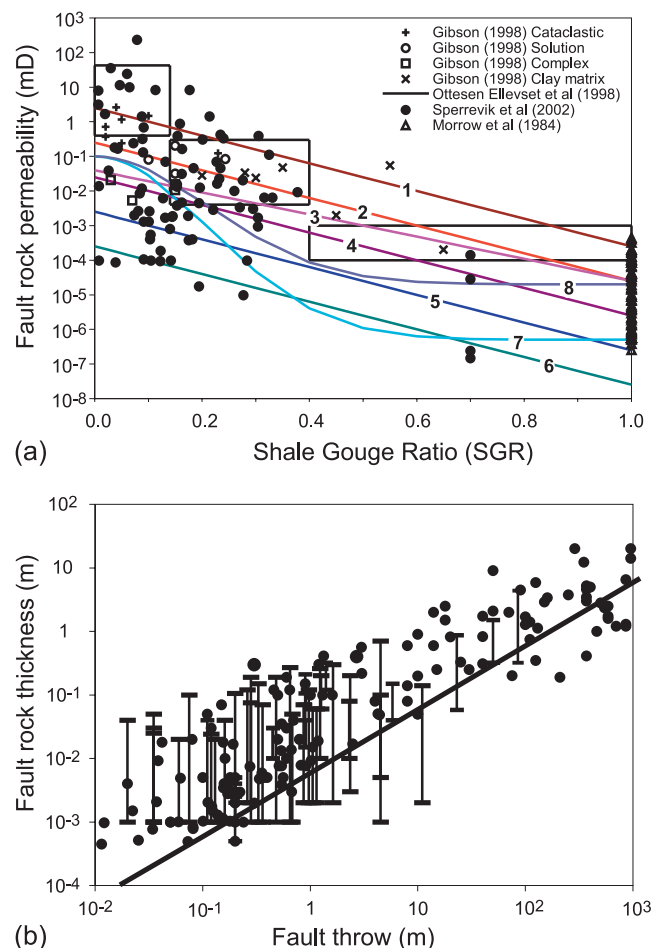


Fig. 4. Fault-rock properties. (a) Fault-rock permeability is calculated as a function of fault shale gouge ratio (SGR) using the eight relationships indicated. Data points show published laboratory measurements (Morrow *et al.* 1984; Gibson 1998; Ottesen Ellevset *et al.* 1998; Sperrevik *et al.* 2002). (b) Fault-rock thickness is modelled as a constant fraction of fault throw (black line). The data show measurements from natural faults. Where several samples have been measured on the same fault, these are linked by a vertical line.

$$\begin{aligned}
 \text{Case 5: } K_f &= 10^{-2.6 - 4JGR} \\
 \text{Case 6: } K_f &= 10^{-3.6 - 4JGR} \\
 \text{Case 7: } K_f &= 10^{-6.3 + 5.3 \exp(-11JGR^2)} \\
 \text{Case 8: } K_f &= 10^{-4.7 + 3.7 \exp(-11JGR^2)}
 \end{aligned} \quad (3)$$

All models use a single linear relationship between fault-rock thickness (t_f) and fault throw (t), given by $t_f = t/170$ (Fig. 4b). This relationship is representative of the harmonic average thickness of outcrop measurements of fault-rock thickness, the appropriate average for inclusion in a transmissibility multiplier if the correlation length of the variability is assumed to be smaller than the grid-blocks (Manzocchi *et al.* 1999). Although a constant fault-rock thickness predictor is used throughout the modelling to reduce the number of input variables, the significant ratio with respect to flow is the ratio of fault-rock thickness to fault-rock permeability (Manzocchi *et al.* 1999). Hence, the difference in behaviour between, for example, models run with permeability Cases 2 and 4 could represent either a decrease in fault permeability by an order of magnitude, or an increase in fault-rock thickness by the same amount.

For a ninth case (referred to as ‘Case 0’) fault rock is not included in the simulation models (all the fault transmissibility multipliers are set to 1.0) so simulation results using this case consider only the effects of fault juxtapositions.

THE EFFECTS OF FAULTS ON PRODUCTION

This section summarizes and discusses the basic influence of fault structure and fault properties on different measures (peak production rate, recovery factor, discounted reservoir value) of the reservoir performance. Discounted value is given by:

$$V = \int_0^{30} (1 + \beta)^{-t} R_t dt, \quad (4)$$

where R_t is the production rate at time t , and β is the discount factor, typically 0.1 (i.e. 10%) per year.

Reservoir performance has been simulated using four different well configurations, each designed to optimize production for one of the four end-member structures. The well configurations are referred to by the name of the structure they are designed around (A, B, C and U) and contain three vertical water injectors situated close to the oil–water contact, and eight or nine vertical producer wells situated at the crest or midway up the structure. Production has been simulated for up to thirty years, subject to well-specific and field-wide economic cut-offs. Further details are given by Matthews *et al.* (2008).

The behaviour of the nine different fault property cases on a particular geological model produced using a particular well configuration is discussed first. The peak oil production rate is shown to correlate strongly with the fault permeability case used, while the recovery factor is highest in a case with intermediate fault properties. Discounted reservoir value, which places a premium on earlier oil production, shows intermediate behaviour, dependent on the discount factor used.

Focusing on the discounted reservoir value of a large number of reservoir models (the ‘basic’ and ‘fault property’ modelling suites described in Manzocchi *et al.* 2008a, table 3), two heterogeneity factors measured in the static geological models are identified that can be calibrated to the overall effects of the faults. Each reservoir structure, however, requires a different calibration for each well configuration examined. In the next section it is shown that these heterogeneity factors can be estimated from large-scale geological characteristics.

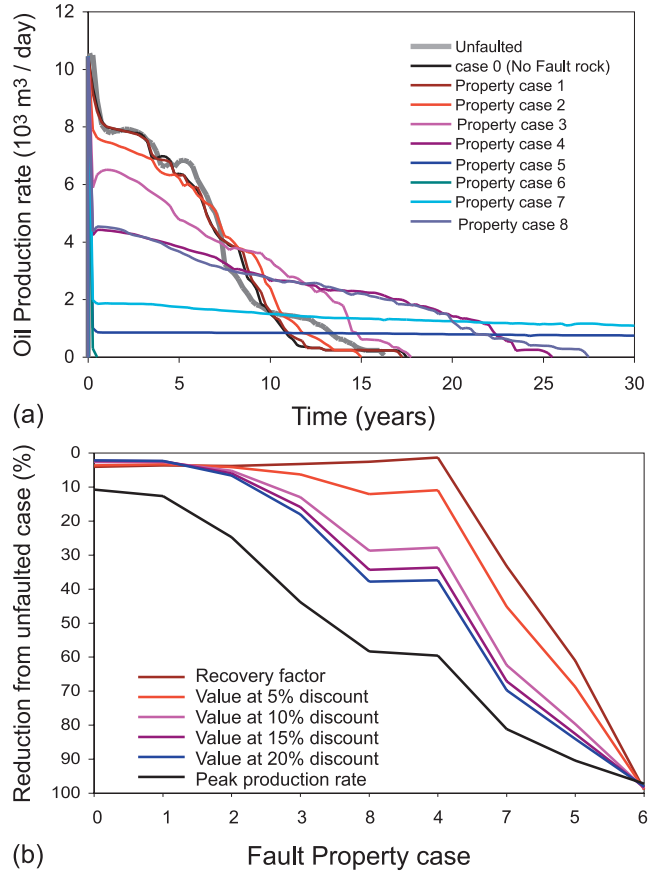


Fig. 5. (a) Oil production rate for the unfaulted and nine faulted versions (fault property cases 0–8) of a particular sedimentological model (number 106, Manzocchi *et al.* 2008a, fig. 6), faulted by structure B2 and simulated using well configuration U. (b) The change in reservoir performance (recovery factor, peak oil production rate and discounted reservoir value at four discount factors) with respect to the unfaulted version of the model, for the nine fault properties cases of this reservoir. Permeability model 0 refers to pure juxtaposition (i.e. no fault rock present).

Whether the calibrations between these factors and the reservoir value can also be deduced is investigated towards the end of the paper.

Behaviour of the faulted models

Figure 5 compares the production behaviour of an unfaulted version of a representative sedimentological model with versions faulted by structure B2 and using each of the nine fault property cases, when simulated using the well configuration designed around the unfaulted model (i.e. well configuration U). In the unfaulted case, production rate stabilizes to a plateau of ≈ 8000 m³ per day within the first ninety days, this rate is maintained for \approx four years, after which it declines rapidly (Fig. 5a). The plateau production rates for the models with no fault rock (Case 0) or the most permeable fault-rock model (Case 1) are very similar to the unfaulted model; however the decline in rate occurs slightly earlier and the recovery factors are lower than in the unfaulted models (Fig. 5b). As the fault property model becomes more severe, the peak production rates decrease, but the field life is extended (e.g. fault property Cases 4 and 8, Fig. 5a). This longer field life results in a gradual increase in recovery factor until fault property Case 4, for which the recovery factor is almost the same as for the unfaulted model (Fig. 5b). Once the faults become even less permeable, both production rate and recovery factors decline rapidly.

It is clear that the field and well production rate cut-off values built into the development plans to increase realism (Matthews *et al.* 2008) have an influence on the recovery factors. Fault property Case 5, for example, has a stable production rate for up to thirty years (Fig. 5a), and could maintain this rate for longer, resulting in a higher recovery factor than recorded. If the well work-overs and economic limits were not present, all models could be run forever and, since all grid-blocks have non-zero permeabilities and no capillary pressure is present in these reservoirs (Matthews *et al.* 2008), all models would eventually have recovery factors representative only of the connate water saturations of the cells. It is therefore more practical from a scientific as well as economic perspective to examine the discounted value of the reservoirs. Since oil produced in the thirtieth year of the field's life is worth less than 5% as much as oil produced in the first year at a 10% discount factor, the arbitrary thirty-year limit placed on the duration of the models has only a very small effect. Figure 5b shows that the discounted reservoir value reflects the behaviour of the peak production rate at higher discount factors, and of recovery factor at lower discount factors.

The trend observed in the models described above is of a decline in plateau production rate as the faults become less permeable, but of an increase followed by a decrease in total oil recovery (Fig. 5b). This behaviour is not peculiar to this reservoir structure, sedimentological model and well configuration. In Figure 6 the fault property cases for a range of faulted sedimentological models simulated with the four well configurations are ranked according to their production rate at ninety days (Fig. 6a), final recovery factor (Fig. 6b) and discounted value at 10% discount factor (Fig. 6c). With the exception of fault property Cases 4 and 8 (which have very similar production rates), there is a consistent trend between the rank of the peak production rate associated with a particular property case across all faulted versions of all sedimentological models and well configurations (Fig. 6a). The relative rankings of the different cases are consistent with a trend in fault permeability assuming a representative SGR value of ϵ 0.23 (Fig. 4a).

The rankings for recovery factor are much more complex (Fig. 6b). The pure juxtaposition model (Case 0), for example, has the best recovery factor in less than 30% of cases and, in over 10% of the cases, it ranks fifth or worse. The rankings for discounted recovery (Fig. 6c) are intermediary between production rate and recovery factor. It therefore appears that reservoirs with lower permeability faults do not necessarily perform more poorly than the same reservoir with more permeable faults.

The change in reservoir value as a function of faults, for this suite of nine sedimentological models simulated with the set of nine fault property cases using well configuration U, is summarized in Figure 7, plotted against fault permeability at the representative SGR value of 0.23. Structure A and C reservoirs show similar behaviour, with little change as a function of permeability if $K_f > 0.1$ mD or $K_f < 0.001$ mD. Effects of fault juxtaposition are higher in structure C reservoirs, with losses in value of up to ϵ 20%. The structure B reservoirs show similar trends to those of structure A if $K_f > 0.1$ mD, but once the fault permeability is low enough to start influencing production, the decline in value with permeability is more rapid, with the highest fault density versions of the structure B reservoirs becoming worthless (at least with this well configuration) when $K_f < 0.0001$ mD. These trends are described more quantitatively below.

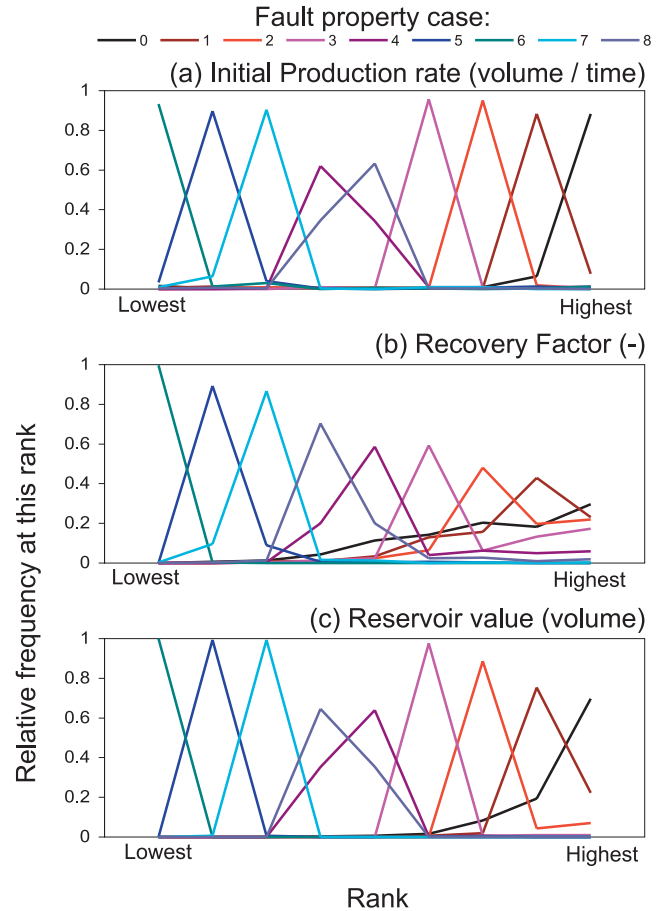


Fig. 6. Rankings of (a) initial production rate, (b) recovery factor and (c) value at 10% discount factor, as a function of the fault property case, for the nine structural versions of nine sedimentological models using all four well configurations (342 models in each fault property case).

Parameterizing the effect of fault juxtaposition

Even if fault rocks are not detrimental to flow, faults influence production by juxtaposing different reservoir units. This section concerns the empirical definition of a model for predicting the percentage reduction in discounted value of a reservoir from its unfaulted state owing purely to fault juxtaposition, a measure termed P_f . A juxtaposition function (J_f) measured from the static geological models is found to provide a reasonable basis for estimating the reduction in value of the reservoirs. The function is defined by:

$$J_f = 1 - \frac{A_f T_f + (1 - A_f) T_{NF}}{T_{NF}} \quad (5)$$

where A_f is the fractional area of faulted connections present in the model (reported in Table 2) and T_{NF} and T_f are the area-weighted arithmetic averages of the grid-block centre to grid-block centre transmissibilities of unfaulted and faulted connections, respectively. A J_f value of zero implies that the juxtaposed permeabilities across faults are no different to the average horizontal permeability of the model. Note that J_f is not a transportable parameter since it depends on the discretization of the grid-blocks through the A_f term. As a general rule, the total number of connections in a model increases more rapidly than the total number of faulted connections as the grid-blocks become smaller, hence J_f will be lower in higher

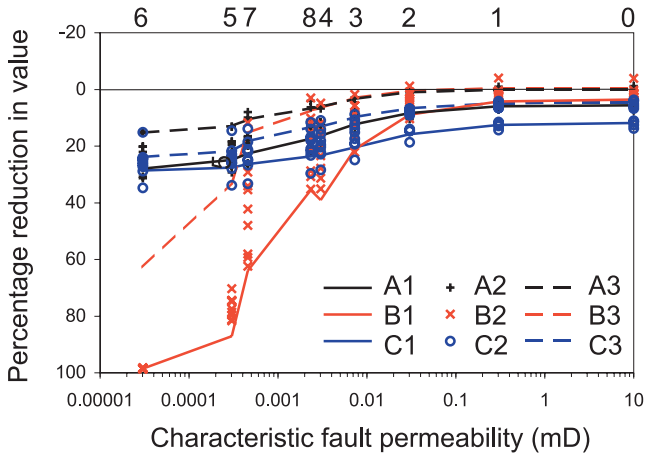


Fig. 7. Percentage reduction in reservoir value (using a 10% discount factor) from the unfaulted state for the nine different structures using well configuration U. The high and low fault density levels (i.e. Codes 1 and 3, respectively) are reported as lines showing the average behaviour of different sedimentological models, while the symbols show results from individual reservoirs containing the intermediate fault density (Code 2). The eight fault property cases that include fault rock are assigned a fault permeability at a representative SGR value of 0.23. Fault property model 0 is assigned a nominal permeability of 10 mD. The fault property cases are shown above the graph.

resolution models. All models considered in this work have the same grid-block sizes (75 m × 75 m × 4 m).

Figure 8 shows the juxtaposition function (J_F) plotted against the reduction in reservoir value as a function of juxtaposition (P_j) for the 12 combinations of fault structure and well configuration. P_j is a roughly linear function of J_F , but the constants defining the function are dependent on both the

particular structure present and on the well configuration used. In some cases (most commonly of structure A and B models) the faulted value is greater than the unfaulted value (i.e. P_j is negative). Juxtaposition has a much more detrimental effect on the value of the structure C reservoirs, and the correlations for these reservoirs are defined better. For all three structures, the effect of juxtaposition is lowest in the case where the well configuration designed around the structure is used (e.g. of the four configurations used on structure C reservoirs, faults have the smallest impact when well configuration C is used). This implies that the wells are well positioned, since the objective of the configuration is to maximize recovery given the particular fault structure it is designed around (Matthews *et al.* 2008).

Parameterizing the effects of fault-rock properties

Fault juxtaposition reduces the value of the reservoirs by a percentage P_j , discussed above. Addition of fault rock may reduce the value by a further percentage termed P_R . A second heterogeneity factor (H_F) measured in the static models captures the effects of fault rock. H_F is given by (Manzocchi *et al.* 1998):

$$H_F = 1 - \frac{K_H}{K_M} \quad (6)$$

where K_M is the reservoir permeability ignoring fault rock, and K_H is the harmonic average permeability of the fault and reservoir rocks. H_F has been measured in the static simulation models using:

$$H_F = 1 - \frac{1}{T_{NF} \left[\frac{A_F}{T_F} + \frac{(1 - A_F)}{T_{NF}} \right]}, \quad (7)$$

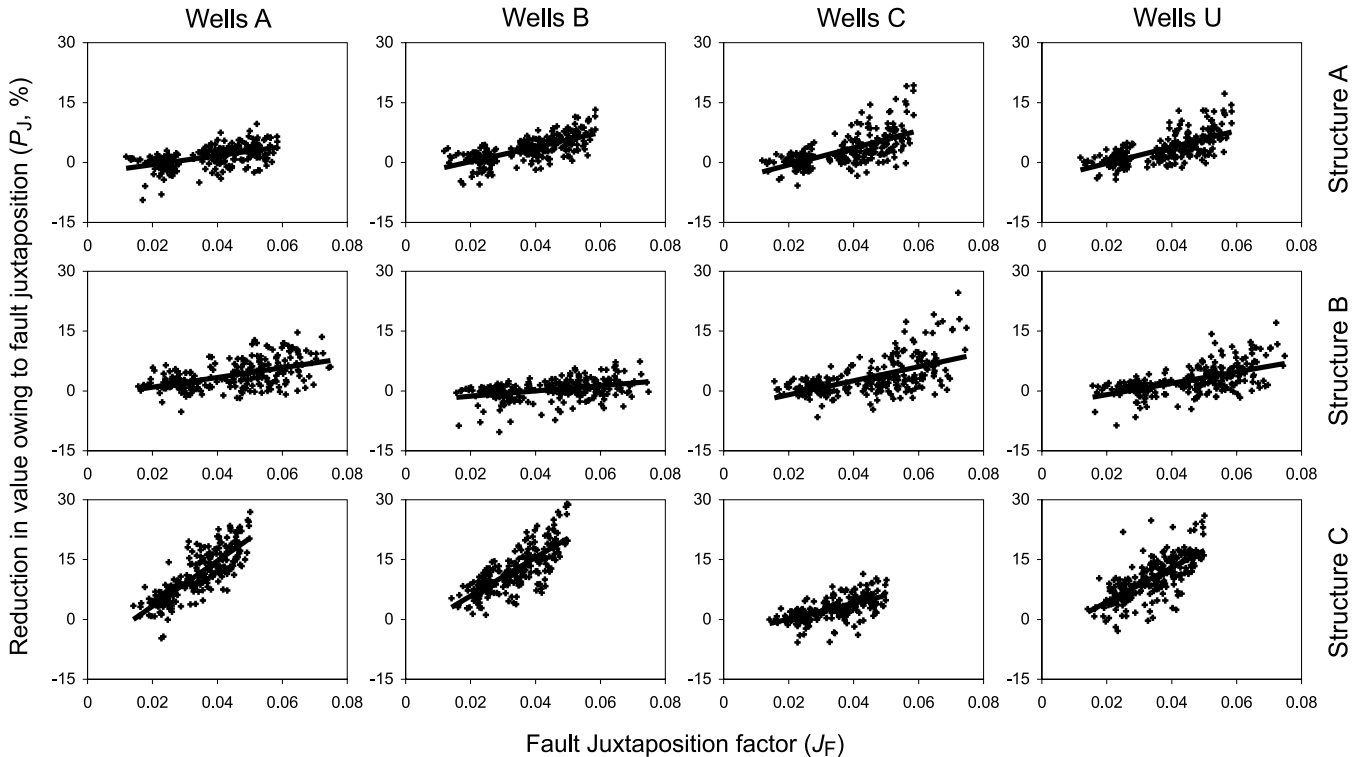


Fig. 8. The percentage reduction in value as a function of fault juxtaposition (P_j) vs. the measured juxtaposition function (J_F) separated into combinations of well configuration and model structure. Each graph contains results from 243 models (81 sedimentological models at three strain levels). The black lines show the best-fit linear correlations.

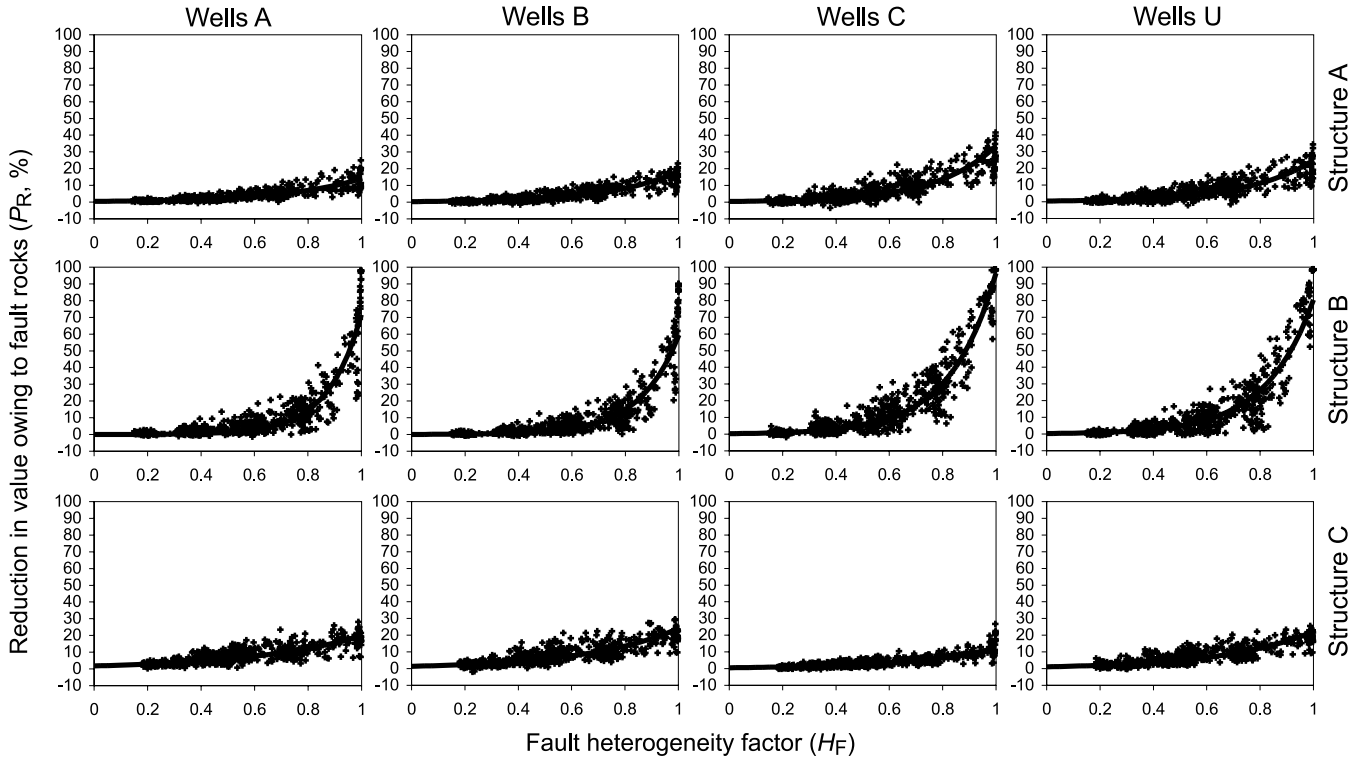


Fig. 9. The percentage reduction in value as a function of fault-rock properties (P_R) vs. the measured heterogeneity function (H_F) separated into combinations of well configuration and model structure. Each graph contains 864 data ([72 sedimentological models \times 3 fault properties+9 sedimentological models \times 8 fault properties] \times 3 strain levels). The black lines show the best-fit exponential correlations.

where T_F (the area-weighted average cell-centre to cell-centre transmissibility of faulted connections) now includes the presence of fault rock. Figure 9 shows cross-plots of H_F against P_R for each well configuration/structure combination, with a best-fit correlation of the form $P_R = c_1 \exp(c_2 H_F)$ (c_1 and c_2 are constants).

Manzocchi *et al.* (1998) introduced H_F as a means of combining gouge density (d_G , i.e. the fraction of a rock volume occupied by low permeability fault rock) and the fault and reservoir permeabilities into a single parameter, for assessing the circumstances in which fault geometry is a significant control on effective permeability. Fault-system geometry has little influence on effective directional permeabilities when H_F is less than about 0.5, since either the fault density is too low, or the ratio of fault to reservoir permeability is too high, for the faults to be a significant heterogeneity (Manzocchi *et al.* 1998). This is manifest in Figure 9, which shows that the curves diverge only when $H_F > 0.5$. Fault rock reduces the reservoir value by less than 10% in all models with $H_F < 0.5$. When $H_F > 0.5$, the geometry of the fault system becomes increasingly important, as the preferred flow paths in the reservoir are now tortuous ones around faults and, by definition, flow around faults is impossible if the fault system is compartmentalized. Hence, P_R at higher values of H_F is much greater for the compartmentalized reservoirs (structure B) than the other two structures.

In structure A reservoirs, fault rocks reduce the value by up to 10–20% (compared to 5–10% due to juxtaposition alone; Fig. 8), while in the compartmentalized structure B reservoirs, sealing faults ($H_F = 1.0$) cause a median reduction in value of \approx 50% when well configuration A or B is used, or \approx 80% with well configuration C or U. The largest P_R for structure C reservoirs is only \approx 20%, comparable with the effects of pure juxtaposition in these reservoirs.

Combining effects of juxtaposition and fault rock

For any particular reservoir, the percentage reduction in value as a function of faults (P_F) combines reductions owing to juxtaposition (P_J) and to fault rocks (P_R) and is given by:

$$P_F = \frac{(V_F - V_{NF})}{V_{NF}} = P_J + P_R - \frac{P_J P_R}{100}, \quad (8)$$

where V_F and V_{NF} are the values of the faulted and unfaulted reservoirs. Figure 10 compares P_F observed in 10 692, four-parasequence flow simulation models, with P_F estimated using the calibrations against measured values of J_F and H_F discussed above. The variability in response shown in Figure 10 is expressed as a running tally of the standard deviation of the prediction. This variability is approximately linear as a function of P_F and represents a signal-to-noise ratio of \approx 5.

Figure 11 identifies the geological sources of the variability in estimated P_F . There does not appear to be any systematic bias as a function of any of the four input sedimentological variables (Fig. 11a–d), three input structural variables (Fig. 11e–g) or the well configurations (Fig. 11h). The most significant trend observed is of an increase in imprecision for the models in which faults have a larger effect (either through higher fault density (Fig. 11f) or lower fault permeability (Fig. 11g)), but at each level the distribution in error remains unbiased.

Summary

Simulation results in this section have been used to calibrate the observed percentage reductions in discounted reservoir value owing to faults (P_F), to geometry and permeability-dependent functions measured in the static flow models (J_F and H_F). Each combination of structure and well configuration requires separate calibration to the two functions. An examination of the

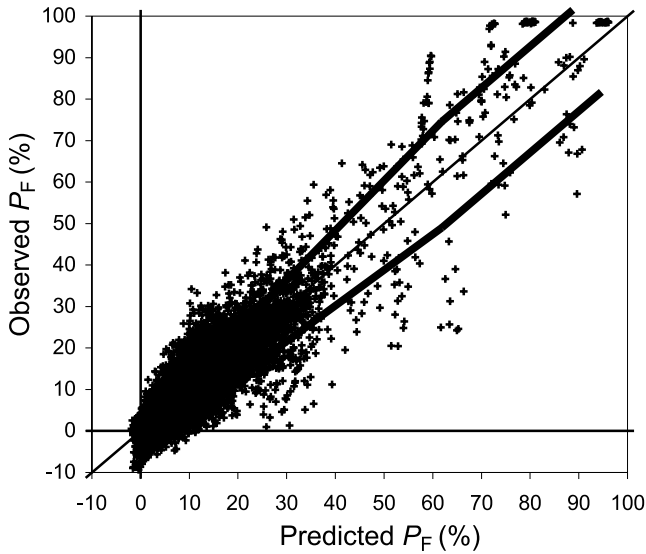


Fig. 10. Percentage reduction in value as a function of faults (P_F , encompassing both juxtaposition and fault-rock effects) observed in the simulation models, vs. the prediction from the calibrations shown in Figures 8 and 9. The thinner line shows the mean prediction, and the thicker lines are ± 1 standard deviation of the predicted value.

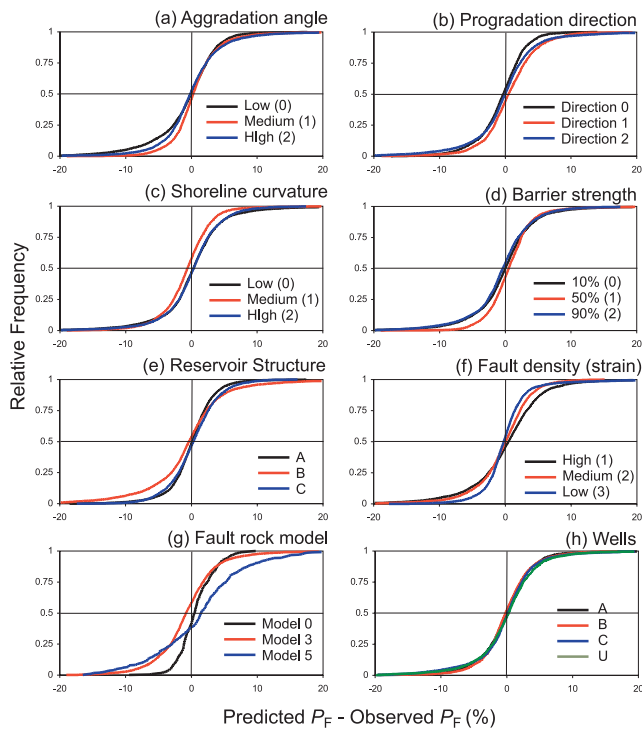


Fig. 11. Frequency distributions of the error in predicted P_F from Figure 10 as a function of each basic input variable: (a) aggradation angle, (b) progradation direction (see Manzocchi *et al.* 2008a for definitions of the codes); (c) shoreline curvature; (d) barrier strength; (e) reservoir structure; (f) fault density level; (g) fault property model; (h) well configuration.

deviation of the modelled responses from the observed reduction in value as a function of the overriding sedimentological and structural model characteristics indicates that the calibrations provide an unbiased estimate of P_F , with a signal-to-noise ratio of 5.

The functions J_F and H_F used in the calibrations were measured using the precise fault connection and grid-block

properties measured in each static simulation model. The following section investigates whether these parameters can be estimated from the overriding geological characteristics of the models. Since these functions strongly influence the production behaviour of the faulted reservoirs, their estimation from basic geological factors would represent a step towards quantitatively predicting the likely effects of faults in reservoirs with different geological characteristics.

PREDICTION OF THE JUXTAPOSITION AND HETEROGENEITY FUNCTIONS

The previous section demonstrated systematic changes in discounted reservoir value as a function of fault system and fault property characteristics. These changes are functions of the well configuration, the basic reservoir structure, and two factors (J_F and H_F) measured in the static models. Calibrations between these parameters give unbiased estimates of the change in reservoir value with a signal-to-noise ratio of 5. This and the next section examine whether these findings can be made more generic and transportable by (a) estimating the two factors from top-level geological characteristics (this section), and (b) estimating the calibrations from basic geometrical and reservoir engineering idealizations (the next section).

Across-fault connectivity is a complex function of fault and sedimentological characteristics (e.g. Bailey *et al.* 2002; James *et al.* 2004; Manzocchi *et al.* 2007) and is best understood in idealized systems. The flow behaviour of the present models is dominated by the most permeable facies present (the upper shoreface; USF) and the following treatment therefore assumes that the crucial controls on J_F and H_F relate to this facies, while ignoring the others. J_F and H_F estimated as a function of a generalization of the geometrical distribution of the USF facies based on this assumption are shown to provide a reasonable match to those measured in the static models.

Figure 12a shows a 2D idealization of the upper shoreface in a parallel shoreline, six-parasequence model with a relatively low aggradation angle. A vertical fault with a constant throw striking parallel to the sedimentological progradation direction will offset the sequence shown on the near face of the block (e.g. Fig. 12b, c) and the fraction of the total USF cross-sectional area which is juxtaposed against USF across the fault ($A_{J,USF}$) is a function of the fault throw and the sedimentological variables indicated on Figure 12a. Figure 12d charts $A_{J,USF}$ as a function of fault throw for a six-parasequence model at two aggradation angles. In the low aggradation angle case (0.2°), connectivity is lost rapidly with increasing throw and reaches a minimum at slightly less than half the parasequence thickness. It then increases again, to reach a maximum at a throw slightly less than the parasequence thickness. At higher throws the same pattern is repeated, with the connectivity maxima becoming less marked. Both the periodicity and the variability of the connectivity decrease at higher aggradation angles and $A_{J,USF}$ as a function of fault throw becomes a smoother function (Fig. 12d).

A vertical fault with a constant throw striking perpendicular to the sedimentological progradation direction will offset a sequence that depends on the precise location of the fault. However, if the fault has a random location, then the most likely $A_{J,USF}$ across the fault is the same as $A_{J,USF}$ of a fault of the same throw striking parallel to the progradation direction. Similarly, the most likely connectivity of a variable throw fault in any orientation is the average of the $A_{J,USF}$ values along the length of the fault, and the same applies for the average connectivity in a system of faults.

A separate connectivity vs. throw curve (e.g. Fig. 12d) has been determined for each aggradation angle (using the central

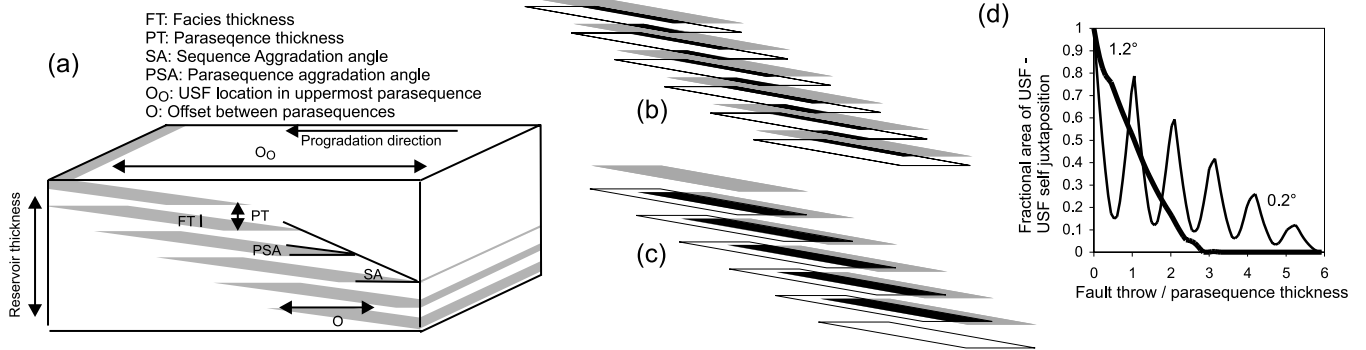


Fig. 12. (a) Idealization of the upper shoreface (USF) facies for a parallel shoreface, six-parasequence model. (b, c) Footwall (grey) and hanging-wall (outlined) USF sequences for a fault with a throw of $c = 0.35$ times (b) and 0.8 times (c) the parasequence thickness. The area of USF-USF juxtaposition in each case is highlighted in black. (d) Fraction of the total USF cross-sectional area juxtaposed against USF as a function of throw, for high (1.2°) and low (0.2°) parasequence aggradation angles (PSA). Note that in these models the offset (O) is varied to maintain an approximately constant system aggradation angle (SA) irrespective of the parasequence aggradation angle (Howell *et al.* 2008).

values of the distributions of relevant sedimentological variables) in the two-, four- and six-parasequence models. These have been combined with the length and throw distributions of the faults in each of the nine fault systems (Fig. 3) to derive an average value of $A_{J,USF}$ for each idealized faulted sedimentological model. Figure 13a shows these results for the high (A1, B1, C1) and low (A3, B3, C3) fault density versions of the four parasequence models, and indicates that the fault system is more significant than the sedimentological variables in defining the average USF-USF connectivity. For the high aggradation angle models, for example, the expected average $A_{J,USF}$ varies from 20% of the average USF cross-sectional area in system C1, to 60% in system B3.

For the geometrical simplifications considered, the average transmissibility of unfaulted reservoir connections (T_{NF} in equations (5) and (7)) is given by the product of the USF transmissibility (on average $850b$ mDm where $b=4$ m; the grid-block thicknesses) and the fraction of the model comprising the USF facies (NTG_{USF} , which is a function of the idealized sedimentological model, Fig. 12a). In the absence of fault rock, and using the assumption that all facies other than the USF are considered impermeable, the average transmissibility of faulted connections (T_F) is estimated by $T_F = T_{NF} A_{J,USF}$. The other variable in equation (5) is the fraction of horizontal cell connections that are faulted (A_F), which is a constant for the each of the nine structures (Table 2). Replacing these terms in equation (5) produces an estimate of J_F as a function of the fault system and the expected aggradation angle:

$$J_F \approx A_F (1 - A_{J,USF}). \quad (9)$$

Figure 13b shows this estimate is fairly robust, although with a tendency to over-predict J_F at higher values.

For the heterogeneity factor (H_{F3} , equation (7)) the T_F term includes fault rock, hence estimates of the fault-rock thickness and permeability need to be included in the simplified assumptions. The fractional volume of the USF facies comprising fault rock (i.e. gouge density, d_G) is the same as the fractional volume of fault rock in the entire model, and, since fault-rock thickness is a constant fraction of throw, is given by $d_G = s/170$, where s is the strain (equation (1)) of the model.

An SGR value is calculated at each corner of each USF-USF connection in the idealized geometrical model (Fig. 12b, c) based on the representative thicknesses and V_{shale} values of the facies overlying and underlying the USF facies. These connection corner SGR values are then averaged across individual

connections and then between all connections to provide an overall estimate of average SGR over the connection area $A_{J,USF}$ (Fig. 13c). This is then converted to a representative fault-rock permeability ($K_{f,USF}$) using the appropriate fault permeability function for the property case considered (equations (3); Fig. 4a). The faulted transmissibility term in equation (7) is then estimated by:

$$T_F \approx \frac{NTG_{USF}}{\frac{d_G}{K_{f,USF}} + \frac{(1-d_G)}{K_{USF} A_{J,USF}}}. \quad (10)$$

Applying this term into equation (7) gives an estimate of H_F in each model as a function of the idealized sedimentology of the system, the fault property case considered and the fault throw population. Figure 13d, which compares the predicted and measured values of H_{F3} , indicates a fairly good match, though with a tendency to under-predict H_F for $H_F < c = 0.6$.

PREDICTION OF THE EFFECTS OF FAULTS ON RESERVOIR VALUE

In the previous section it was shown that the juxtaposition and heterogeneity functions (J_F and H_{F3} respectively), which correlate with the change in reservoir value on the inclusion of faults (Figs 8 and 9), can be estimated from large-scale structural and sedimentological reservoir characteristics, given the facies proportions and the fault-rock permeability and thickness predictions. This section examines whether the form of the calibrations themselves can be estimated. Conceptualizations from 2D streamline theory (e.g. Craig 1971) have been used to consider what the effects on the sweep efficiency and production rates of faults in different orientations are likely to be. A generalized model derived from these considerations is developed to link directional permeabilities with discounted value, and calibrated to the simulation results of the unfaulted reservoirs. An empirical 2D model for the fractional permeability of a system containing low permeability faults (Manzocchi 1997) is then applied to calculate input parameters to the streamline model. Inclusion of 3D juxtaposition effects and of economic thresholds built into the production plans is necessary before the resultant predictor can be applied to estimate the differences in discounted value between unfaulted and faulted versions of the models.

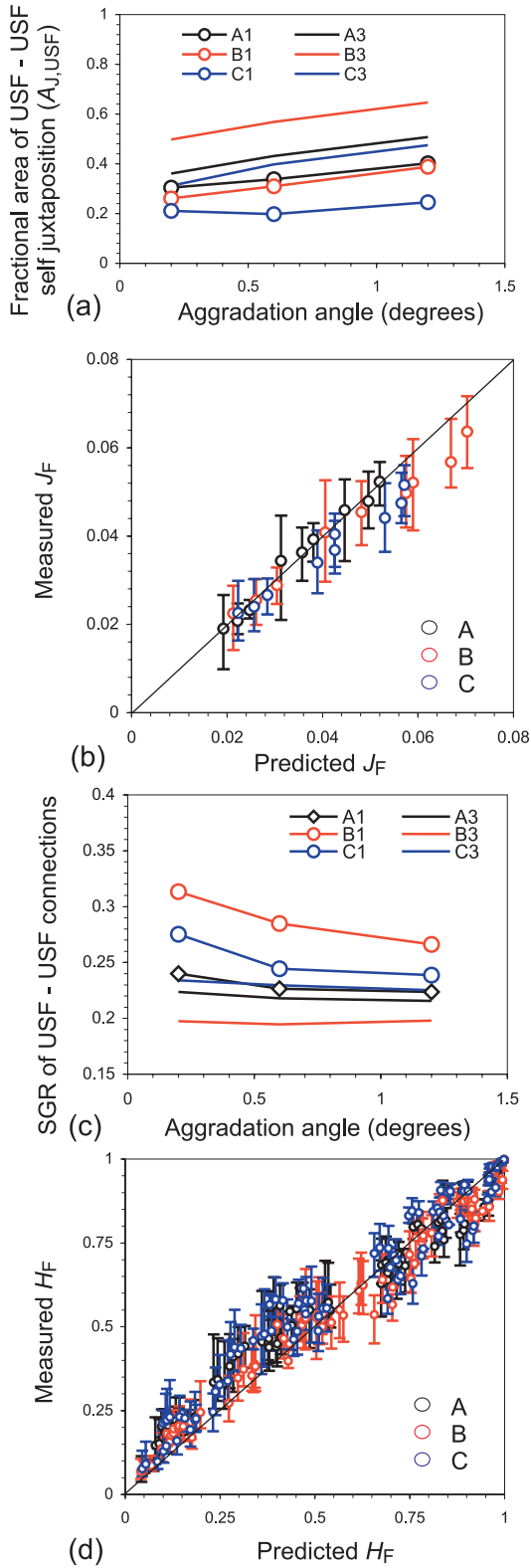


Fig. 13. (a) Expected fraction of the total USF cross-sectional area juxtaposed against USF for four-parasequence models as a function of aggradation angle for the high and low fault density structural models. (b) Measured vs. estimated juxtaposition function (J_F). The error bars represent the range in J_F measured in 27 sedimentological models for which the same value is predicted. (c) Expected shale gouge ratio of USF-USF connections, for the four-parasequence models as a function of aggradation angle for the high and low fault density structural models. (d) Measured vs. predicted heterogeneity function (H_F). The error bars represent the range in H_F measured in between 2 and 27 sedimentological models for which the same value is predicted.

Effects of permeability anisotropy on 2D sweep efficiency and flow rate

A streamline is a line following the velocity field between injector and producer wells. Streamlines may be generated by solving Laplace's equation,

$$\nabla^2 \phi = 0 \quad (11)$$

where ϕ is the potential, and a series of sources and sinks corresponding to the desired pattern of injectors and producers completes the description of the problem.

In two dimensions (X and Y) perpendicular to gravity, Laplace's equation reduces to

$$\frac{\partial^2 \phi}{\partial X^2} + \frac{\partial^2 \phi}{\partial Y^2} = 0, \quad (12)$$

where ϕ is synonymous with pressure. The underlying flow equation,

$$\nabla K \nabla \phi = 0 \quad (13)$$

allows a problem with anisotropic permeability to be transformed into a problem with isotropic properties, but having different dimensions. The flow equation in two dimensions (where K_X and K_Y are in the principal plan-view orthogonal directions),

$$K_X \frac{\partial^2 \phi}{\partial X^2} + K_Y \frac{\partial^2 \phi}{\partial Y^2} = 0, \quad (14)$$

can be transformed into the equation

$$\frac{\partial^2 \phi}{\partial x^2} + \frac{\partial^2 \phi}{\partial y^2} = 0, \quad (15)$$

where $y=Y$ and $x=X(K_Y/K_X)^{0.5}$. The ratio:

$$K_Y/K_X \quad (16)$$

therefore defines the shape of the streamlines and, hence, the sweep efficiency of the reservoir. If $K_Y/K_X > 1$, the streamlines will be wider and the sweep efficiency of a reservoir will be greater. Conversely, if K_Y is reduced relative to K_X , the permeability anisotropy causes the streamlines to short-circuit on their way from injector to producer, and the sweep is reduced. Hence, structures A and B, in which the faults are predominantly perpendicular to the flow direction, will have a greater sweep efficiency as the faults become stronger barriers to flow. The anisotropy in structure C is in the opposite direction, so $K_X > K_Y$ and the reservoirs have a lower sweep efficiency.

If the ratio K_Y/K_X is constant, the shape of the streamlines is unaltered as the reservoir permeability is lowered; however, the flow rates and, hence, discounted reservoir value, are lower. The value of

$$(K_X K_Y)^{0.5} \quad (17)$$

is approximately proportional to the flow rate that can be achieved with fixed injection and producer pressures in a 2D anisotropic case.

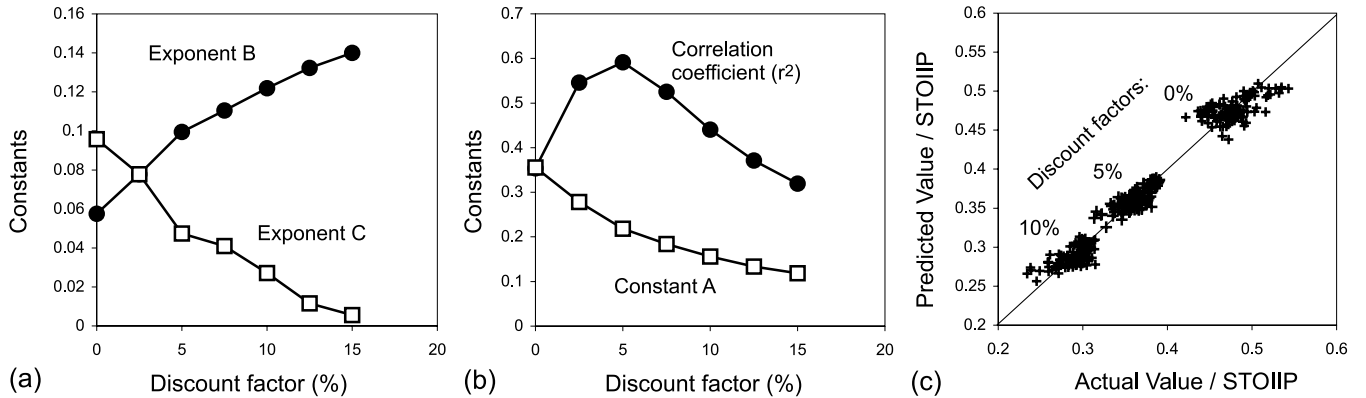


Fig. 14. (a) Best-fit exponents B and C and (b) best-fit constant A , derived from fitting the discounted reservoir value to the streamline model for the unfaulted models simulated using well configuration U. (b) also shows Pearson's correlation coefficients for the fits at the different discount factors. (c) Predicted vs. observed value of the reservoirs from the best-fit expression at the three discount factors indicated. See text for discussion.

Application to the unfaulted models

The implications of the considerations above are that the value of a reservoir should increase as a function of both K_Y/K_X and $(K_X K_Y)^{0.5}$, with the former (relating to sweep efficiency) being more important at lower discount factors and the latter (relating to flow rate) being more significant at higher discount factors. This conceptual model is tested using flow results from 81 unfaulted sedimentological models run on well configuration U (Fig. 14). For each sedimentological model, a bulk K_X and K_Y have been estimated from a pressure solver. A model for discounted reservoir value of the form:

$$V_\beta = A \cdot STOIPP \cdot F_{RATE}^B \cdot F_{SWEEP}^C \quad (18)$$

is assumed, where V_β is the reservoir value at a discount factor β ; A , B and C are constants, $STOIPP$ is the stock-tank oil initially in place (measured in each sedimentological model) and, in accordance with the discussions above, F_{RATE} and F_{SWEEP} are functions related to flow rate and sweep efficiency, respectively, and are given by:

$$F_{RATE} = (K_X K_Y)^{0.5} \quad (19)$$

and

$$F_{SWEEP} = K_Y/K_X. \quad (20)$$

Figure 14 shows the values of A , B and C that provide the best match between the model (equation (18)) and the simulation results at a variety of discount factors. As expected, B increases and C decreases in significance at higher discount factors. The best fit to the model is obtained at a discount factor of 5% (Fig. 14b); however, a reasonable fit is obtained throughout the range of discount factors examined.

Estimation of the sweep and rate functions in the presence of faults

The considerations from streamline theory above have shown that the permeabilities parallel and perpendicular to the water-flood direction, expressed as different functions relating to the sweep efficiency and likely flow rate, can be used in a single function to assess the likely discounted reservoir value given a particular well configuration. Next is a consideration on how the two permeability values (K_X and K_Y) might be deduced in the presence of faults.

Based on extensive flow simulation, Manzocchi (1997) empirically derived equations for defining in 2D the maximum and minimum directional fractional permeabilities of representative networks of low permeability faults as a function of a fault-rock heterogeneity term (H_F), a dimensionless fault density term (d_L) and a fault system anisotropy term (α). A graphical representation of the predictor is shown in Figure 15. These three terms are known for each reservoir considered in the present study: d_L and α are functions of the geometrical fault system characteristics, and have been discussed with reference to Table 2, while H_F is a function of the fault and reservoir permeabilities, and can be estimated from basic fault systems and sedimentological characteristics, as outlined in the previous section. The predictor can therefore be used to estimate the directional permeabilities needed by equations (19) and (20), allowing equation (18) to estimate the discounted value of the faulted reservoirs.

Two further issues must be considered, however. Both the streamline model and the permeability model are two dimensional and, therefore, incapable of taking account of the effects of fault juxtaposition. Secondly, the economic cut-offs built into the production plans mean that wells are abandoned if injection or production rates fall below specified values. Effects of these cut-offs are not contained in equation (18) since the equation is based on unfaulted models for which the producer wells are only deactivated when they exceed allowable water-cut thresholds. Flow rate thresholds can, however, play a role in the simulated production histories of some of the faulted models (Fig. 5a).

Estimation of fault juxtaposition effects

In the absence of 3D effects, the 2D fractional permeability model (Fig. 15) could be applied using the value of α reported in Table 2 to estimate the permeability parallel to the main flow direction (K_X in equations (19) and (20)), and 90 minus this value to give permeability perpendicular to the flow direction (K_Y). These permeability estimates will be too high, since they do not take into account 3D effects of juxtaposition. An attempt to take juxtaposition effects into account is made by assuming that in the presence of open faults, each fault is sealing along its length with the exception of self-juxtaposed USF-USF windows. K_X and K_Y are then calculated from the fractional permeability model using $H_F=1$ (i.e. a value representative of sealing faults) and a revised d_L value which excludes the portions of the faults over which the USF is self-juxtaposed (i.e. the fractional area $A_{J,USF}$ discussed in the previous section). The rate and sweep functions (equations (19) and (20)) calcu-

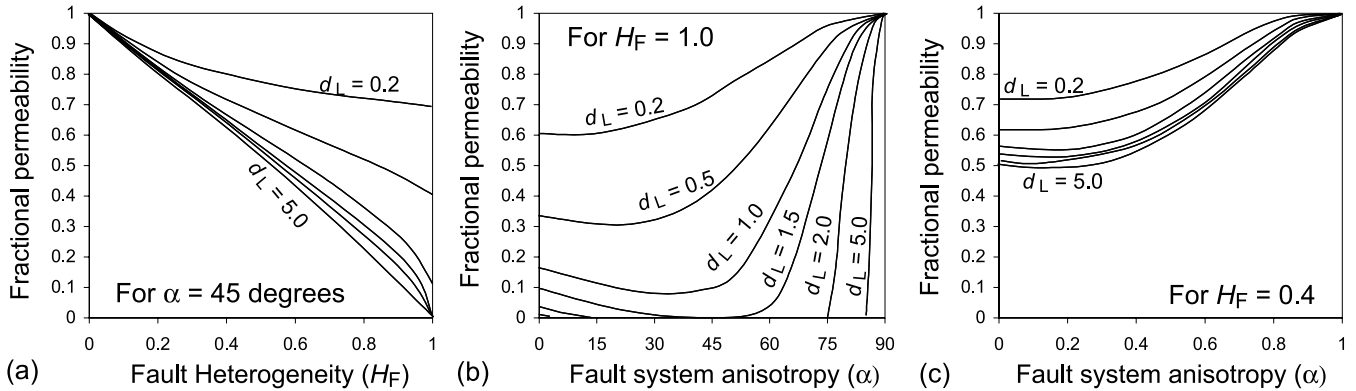


Fig. 15. Model for the fractional permeability of representative 2D networks of low permeability faults, after Manzocchi (1997). (a) Fractional permeability as a function of fault heterogeneity (H_F) for isotropic fault systems ($\alpha=45^\circ$) (b) Fractional permeability as a function of fault system anisotropy (α) for sealing faults ($H_F=1.0$). (c) As (b), but for moderately permeable faults ($H_F=0.4$). All graphs show six values for the line density of faults ($d_L=0.2, 0.5, 1.0, 1.5, 2.0, 5.0$) and are based on random systems for which the percolation threshold in the isotropic case occurs at $d_L=1.56$.

lated with these values are then input into the overall model of reservoir value (equation (18)) to give a value for the faulted reservoir. This is then compared with the value of the unfaulted reservoir calculated using an isotropic permeability equal to $NTG_{USF}K_{USF}$ (see the previous section for a discussion of these terms) to give an estimate of the percentage change in reservoir value as a function of fault juxtaposition (P_j). A comparison between observed and predicted P_j (Fig. 16) shows that this pragmatic attempt to include 3D flow effects using a 2D permeability predictor provides reasonable estimates of the effect of juxtaposition in structure A and C reservoirs, but drastically overestimates P_j in structure B reservoirs.

Once the effects of juxtaposition have been estimated as discussed above, it is necessary to estimate the effects of fault rock. The change in value of the reservoirs from the juxtaposition case owing to the inclusion of fault-rock effects (the term P_R in Figure 9 and equation (8)) is calculated from estimates of K_X and K_Y derived using the values of H_F , d_L and α estimated from the overall geological characteristics of each model. Justification for using a 2D model in this case is easier,

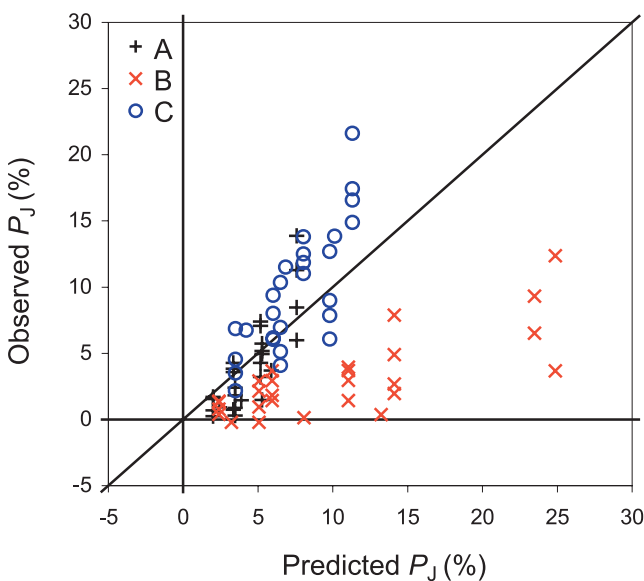


Fig. 16. Observed vs. predicted reduction in value as a function of fault juxtaposition (P_j) following the approximate transformation of the streamline model from 2D to 3D. Twenty-seven cases for each structure. See text for discussion.

since it is assumed that the treatment above takes into account the 3D effects of juxtaposition.

Inclusion of production rate cut-off values

Figure 17a and b show the estimated rate and sweep functions (F_{RATE} and F_{SWEEP}) calculated following the procedures outlined above, plotted against fault-rock permeability for the high and low density versions of each structure, using representative values of sedimentological variables. Structure C reservoirs have the highest rate functions but the lowest sweep functions, consistent with the considerations above. Structure A and B reservoirs have sweep functions >1 , indicative of faults preferentially increasing the sweep efficiency of the reservoir. Both functions are approximately constant for the individual structures when $K_j > 0.3$ mD, at a level representative of the effect of juxtaposition. As discussed above (Fig. 16), the F_{RATE} function in this region is therefore too low for the B structures.

In Figure 17c, the expected reduction in reservoir value is calculated from the F_{RATE} and F_{SWEEP} functions shown in Figure 17a, b. Figure 17c can be compared directly with Figure 7 to establish whether the effects of faults estimated from top-level geological considerations combined with the conceptualizations from streamline theory are similar to the average observed behaviour. The curves are broadly similar, but have two important differences. The first difference is the overestimate of the juxtaposition effect in structure B reservoirs, discussed above. The second difference is the much more modest decline in modelled P_F relative to observed average P_F for the structure B reservoirs with $K_F < 0.001$ mD.

The reason for this latter discrepancy is the absence of economic cut-off values in the model for P_F (i.e. equation (18)) compared to those present in the actual well configuration used for the simulations. In the simulation models, any production well that has an oil production rate lower than a cut-off value of between 50 and 100 m³ per day is shut in (Matthews *et al.* 2008). The peak production rate in the unfaulted models is around 8000 m³ per day (e.g. Fig. 5a) and the average rate function in the unfaulted models is ≈ 220 mD. Well configuration U contains eight producer wells, thus, taking a mean cut-off value of 75 m³ per day, if all wells produced at the same rate they would be expected to become inactive at a field production rate of ≈ 600 m³ per day. For the reservoir permeabilities present this equates to a F_{RATE} value of ≈ 16.5 mD. In reality, the wells will have different production rates, hence will start to become inactive at a higher field production rate. The effect of the

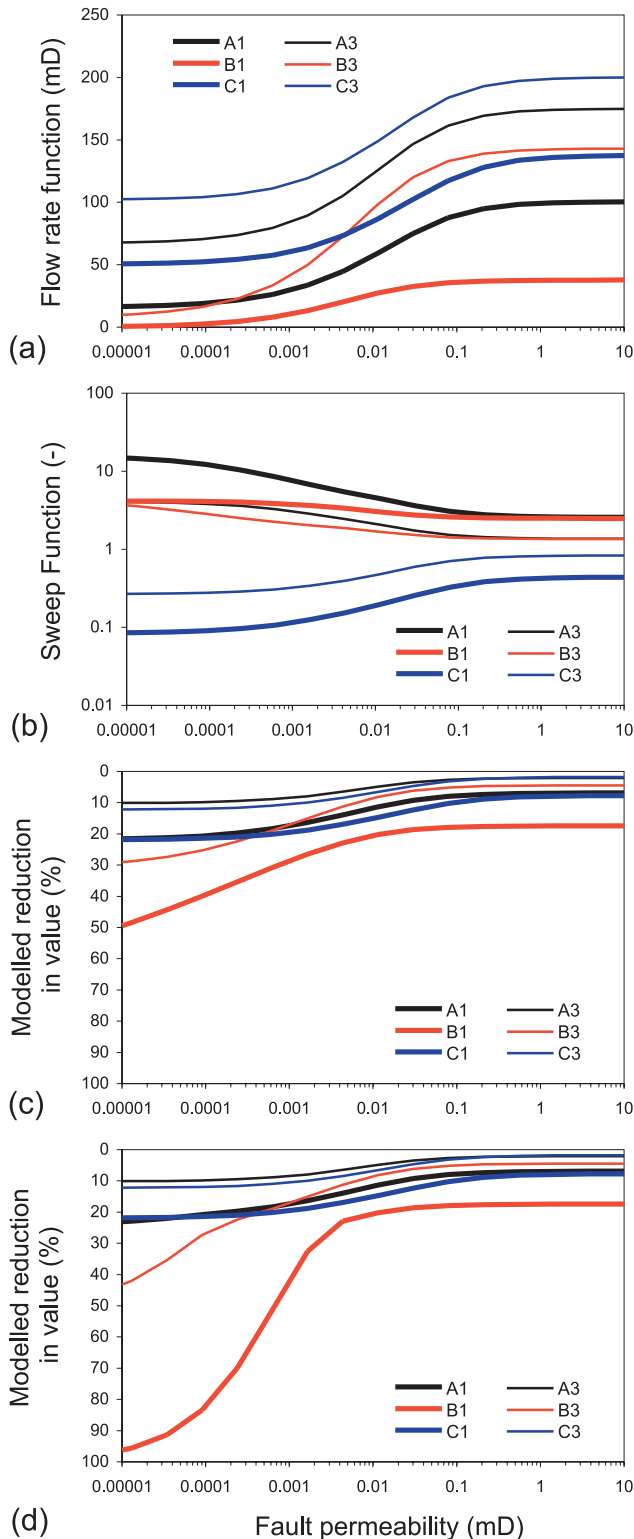


Fig. 17. (a) Flow rate function (F_{RATE}) and (b) sweep function (F_{SWEEP}) predicted for representative sedimentological models for the high density (code 1) and low density (code 3) versions of the three structures (A, B and C). (c, d) Predicted reduction in reservoir value owing to faults (c) ignoring and (d) including the economic considerations. See text for discussion.

cut-offs is included very crudely by multiplying the value of constant A (equation (18)) by $F_{RATE}/20$ if F_{RATE} falls below a cut-off value of 20 mD. The effect of this modification, shown in Figure 17d, changes the curves of the structure B reservoirs,

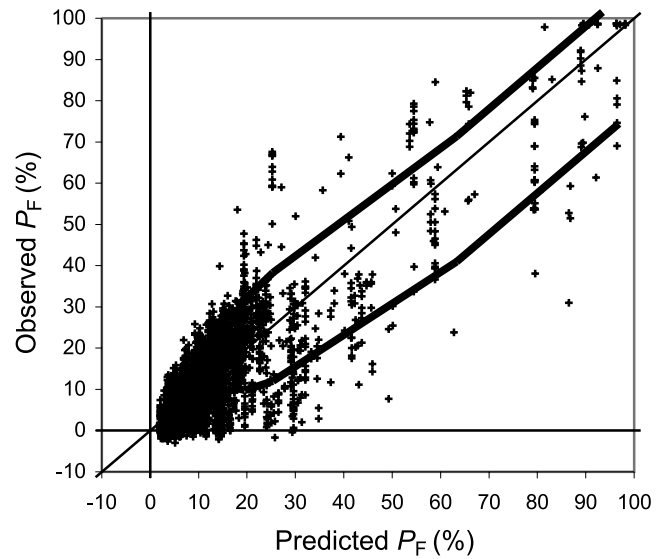


Fig. 18. Percentage reduction in value as a function of fault rock (P_F , encompassing both juxtaposition and fault rock) observed in the simulation models, vs. the prediction from the geological and flow-related idealizations. The thinner line shows the mean prediction, while the thicker lines are ± 1 standard deviation of the predicted value.

making them much more reminiscent of the actual results (Fig. 7) in which the economic controls play an important role in production from these reservoirs when they have less permeable faults.

Performance of the predictor of change in reservoir value

Figure 10 compared the observed percentage reductions in reservoir value (P_F) with the reduction in value obtained by calibrating first the reduction in value due to fault juxtaposition, and then the reduction in value due to fault rocks, to two heterogeneity functions measured in the static models. Separate calibrations were required for each combination of structure and well configuration. The resultant predictions of P_F are unbiased with respect to geological characteristics of the models (Fig. 11) and are subject to a signal-to-noise ratio of ≈ 5 (Fig. 10).

This and the previous sections have been concerned with estimating both the two heterogeneity functions, and the form of the calibrations, from large-scale geometrical model characteristics (i.e. the fault populations present and basic parasequence-scale sedimentological architecture). Figures 18 and 19 show analogous plots to Figures 10 and 11 for the faulted reservoirs simulated with well configuration U, but this time using P_F predicted using these estimates. There is both more variability in response (the standard deviation of the error is $\approx 30\%$ of the prediction as opposed to 20% in Fig. 10), and significant biases as a function of certain model characteristics (Fig. 19). None the less, these results are encouraging. The estimates in Figure 18 are based on only a few simulation models of unfaulted reservoirs that have been used to define the well configuration-specific model for discounted value (Fig. 14; equation (18)), and the remainder of the treatment is based on conclusions from geometrical idealizations of the sedimentology and structure of the reservoirs. It is clear that these idealizations cannot capture the 3D effects of fault juxtaposition entirely; however, plots such as Figure 17 are of quantitative value in assessing the effects of faults on production for the different fault structure cases.

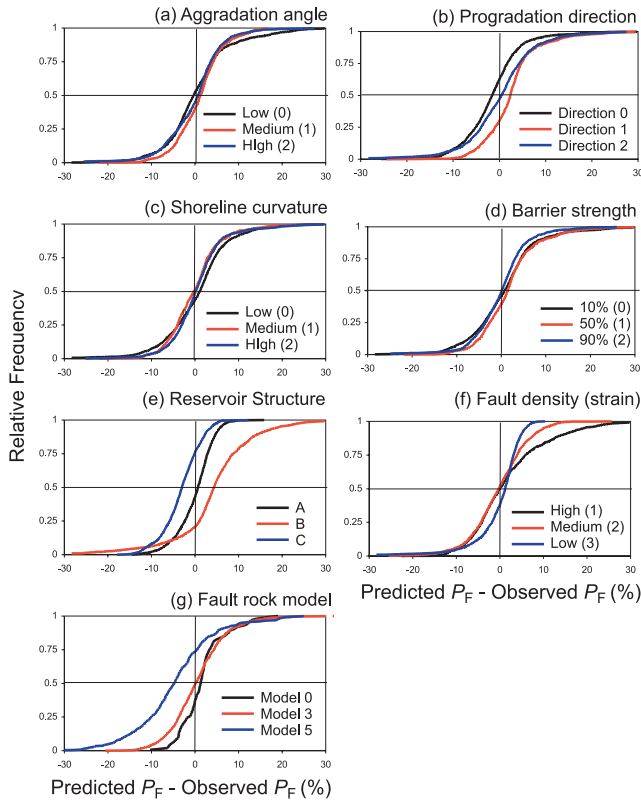


Fig. 19. Frequency distributions of the error in predicted P_F from Figure 18 as a function of each basic input variable: (a) aggradation angle; (b) progradation direction (see Manzocchi *et al.* 2008a for definitions of the codes); (c) shoreline curvature; (d) barrier strength; (e) reservoir structure; (f) fault density level; (g) fault-rock permeability model.

SUMMARY AND CONCLUSIONS

The objective of this work has been to develop methods for understanding and quantifying the influences of fault system properties on oil recovery in shallow-marine reservoirs. The approach taken – to build and simulate production in thousands of geologically distinct reservoir models drawn from a reasonably small geological parameter-space – allows trends in production behaviour to be examined, since a large number of models are required for a quantifiable signal-to-noise ratio. The focus has been on the ‘signal’ portion of this ratio, and unbiased correlations have been established for determining the reduction in economic value of a reservoir as a function of a pair of heterogeneity functions measured in the static simulation models.

The ‘noise’ component of the signal-to-noise ratio is also significant, as it reflects the variability in response arising as a function of reservoir-specific heterogeneities. For example, the fault density level is the strongest factor controlling the changes in reservoir value as a function of fault juxtaposition. However, the variability in response to juxtaposition also increases at larger fault densities. Hence, the uncertainty with which the changes in value as a function of fault juxtaposition can be established increases in absolute terms in proportion to the expected change. It is found that based on the two heterogeneity measures, this uncertainty is $\approx 20\%$ of the prediction. This is consistent with the variation found between different sedimentological realizations of parametrically equivalent SAIGUP models reported by Skorstad *et al.* (2005, 2008).

The quantitative estimates of the loss in reservoir value as a function of faults, discussed in the previous paragraph, derive

from calibrations made independently for each of the 12 combinations of well configurations and gross fault structure. The geometry of the fault system with respect to the principal flow directions in the reservoir is crucial for understanding the effects of faults on production which are varied and often counterintuitive. It is found that higher permeability faults (either without fault rock or using the more permeable ranges of published fault-rock permeability curves) cause the largest decreases in reservoir value when they are aligned parallel to the waterflood direction. This is because faults in this orientation significantly reduce the sweep efficiencies of the reservoirs. Conversely, moderately sealing faults, if orientated perpendicular to the waterflood direction, can increase the value of a reservoir due to increasing sweep efficiency, despite reducing production rates. These effects are both exacerbated if lower discount factors are used to measure the value of the reservoirs. Models with open and sealing faults do not necessarily provide end-member behaviour.

In reservoirs not compartmentalized by faults, the fault-rock permeability estimates are influential on reservoir production only over about a two-orders of magnitude range. At permeabilities above this range, the precise permeability value is unimportant, as the faults are not sufficiently impermeable to impede across-fault flow and the reservoir performance is indistinguishable from a case ignoring fault rocks. At fault permeabilities below this range, the main flow paths are tortuous ones around faults and these are not influenced by the fault permeabilities. In compartmentalized reservoirs, across-fault flow is essential and a rapid reduction in reservoir value is observed once fault permeabilities are sufficiently low for the faults to impede across-fault flow appreciably. The location of the two-orders of magnitude range over which fault permeability is a significant uncertainty on production depends not only on fault permeability, but also on fault-rock thickness and reservoir permeability. These factors can be summarized using the fault-rock heterogeneity factor (H_F) described in this work.

Although based on 2D idealizations, streamline theory, combined with a model for determining 2D directional effective permeabilities as a function of characteristics of fault systems and new methods for estimating the juxtaposition and heterogeneity factors from top-level geological characteristics, has provided a reliable framework for interpreting the results. The main restriction on applying these methods directly has been including the effects of fault juxtaposition. This is a thoroughly 3D problem, and inclusion of estimates of geometrical juxtaposition factors into a predictive framework has relied on some fairly arbitrary (and not very accurate) 2D to 3D transformation assumptions. Despite this, existing analytical treatments based on 2D idealizations of flow or fault systems have proved useful for interpreting quantitatively the behaviour of the faulted reservoirs. The conceptualizations and tools described in this study should therefore be transportable outside the model parameter space used in this study.

The study demonstrates that predicting the effects of fault juxtaposition is significantly more problematical than predicting the effects of fault rock. An accurate representation of fault throws is therefore essential in models used for testing the production efficiency of different well placement plans, and the robustness of the chosen plan should be tested explicitly against uncertainties in fault throws. Uncertainties in fault-rock properties, by contrast, may have very little effect on production uncertainty, since the uncertainty in fault properties may be entirely contained one side or the other of the two-orders of magnitude region over which changes in fault permeability can alter the predilection for across-fault, as opposed to around-fault, flow.

The European Commission partly funded SAIGUP under the EU Fifth Framework Hydrocarbons Reservoir Programme. Patrick Corbett and Quentin Fisher are thanked for reviews. We are very grateful to Badley Geoscience, BG International, Roxar and Shell for their support of the SAIGUP project and for their sponsorship of the production of this thematic set.

REFERENCES

- Bailey, W.R., Manzocchi, T., Walsh, J.J. *et al.* 2002. The effect of faults on the 3-D connectivity of reservoir bodies: a case study from the East Pennine Coalfield, U.K. *Petroleum Geoscience*, **8**, 263–277.
- Blehaut, J.F., Beek, F. van, Billeau, C. *et al.* 1999. Shearwater prospect development: a high pressure/high temperature challenge. In: Fleet, A.J. & Boldy, S.A.R. (eds) *Petroleum Geology of Northwest Europe: Proceedings of the 5th conference*. Geological Society, London, 1021–1028.
- Bonnet, E., Bour, O., Odling, N.E., Davy, P., Main, I., Cowie, P. & Berkowitz, B. 2001. Scaling of fracture systems in geological media. *Reviews of Geophysics*, **39**, 347–383.
- Bour, O. & Davy, P. 1997. Connectivity of random fault networks following a power-law length distribution. *Water Resources Research*, **33**, 1567–1583.
- Childs, C., Manzocchi, T., Nell, P.A.R., Walsh, J.J., Strand, J.A., Heath, A.E. & Lygren, T.H. 2002. Geological implications of a large pressure difference across a small fault in the Viking Graben. In: Koestler, A.G. & Hunsdale, R. (eds) *Hydrocarbon Seal Quantification*. Norwegian Petroleum Society Special Publications, **11**, 127–139.
- Craig, F.F. 1971. The reservoir engineering aspects of waterflooding. *SPE Monograph Series*, **3**, 12–44.
- Crawford, B. R., Myers, R. D., Woronow, A. & Faulkner, D. R. 2002. Porosity–permeability Relationships in Clay-bearing Fault Gouge. Paper SPE/ISRM78214, presented at the SPE/ISRM Rock Mechanics Conference, Irving, Texas, 20–23 October.
- Gibson, R.G. 1998. Physical character and fluid-flow properties of sandstone derived fault gouge. In: Coward, M.P., Daltaban, T. & Johnson, H. (eds) *Structural Geology in Reservoir Characterisation*. Geological Society, London, Special Publications, **127**, 83–97.
- Howell, J.A., Skorstad, A., MacDonald, A., Fordham, A., Flint, S., Fjellvoll, B. & Manzocchi, T. 2008. Sedimentological parameterization of shallow-marine reservoirs. *Petroleum Geoscience*, **14**, 17–34.
- James, S., Pronk, D., Abbots, F., Ward, V., van Dierendonk, A. & Stevens, D. 1999. The Brent Field: improving subsurface characterization for late field life management. In: Fleet, A.J. & Boldy, S.A.R. (eds) *Petroleum Geology of Northwest Europe: Proceedings of the 5th conference*. Geological Society, London, 1039–1050.
- James, W.R., Fairchild, L.H., Nakayama, G.P., Hippler, S.J. & Vrolijk, P.J. 2004. Fault-seal analysis using a stochastic multifault approach. *American Association of Petroleum Geologists Bulletin*, **88**, 885–904.
- Jian, F.X., Larue, D.K., Castellini, A. & Toldi, J. 2004. Reservoir modeling methods and characterization parameters for a shoreface reservoir: what is important for fluid flow performance. *SPE Reservoir Evaluation and Engineering*, **April**, 89–103.
- Larue, D.K. & Legarre, H. 2004. Flow units, connectivity and reservoir characterization in a wave-dominated deltaic reservoir: Meren Reservoir, Nigeria. *American Association of Petroleum Geologists Bulletin*, **88**, 303–324.
- Manzocchi, T. 1997. *Flow impairment in faulted sandstone reservoirs*. PhD thesis. Heriot Watt University.
- Manzocchi, T. 2002. The connectivity of two dimensional networks of spatially correlated fractures. *Water Resources Research*, **38**, 1162 (doi:10.1029/2000WR000180).
- Manzocchi, T., Ringrose, P.S. & Underhill, J.R. 1998. Flow through fault systems in high porosity sandstones. In: Coward, M.P., Johnson, H. & Daltaban, T.S. (eds) *Structural Geology in Reservoir Characterization*. Geological Society, London, Special Publications, **127**, 65–82.
- Manzocchi, T., Walsh, J.J., Nell, P. & Yielding, G. 1999. Fault transmissibility multipliers for flow simulation models. *Petroleum Geoscience*, **5**, 53–63.
- Manzocchi, T., Walsh, J.J., Tomasso, M., Strand, J., Childs, C. & Haughton, P. 2007. Static and dynamic connectivity in bed-scale models of faulted and unfaulted turbidites. In: Jolley, S.J., Barr, D., Walsh, J.J. & Knipe, R.J. (eds) *Structurally Complex Reservoirs*. Geological Society, London, Special Publications, **292**, 309–336.
- Manzocchi, T., Carter, J.N., Skorstad, A. *et al.* 2008a. Sensitivity of the impact of geological uncertainty on production from faulted and unfaulted shallow marine oil reservoirs: objectives and methods. *Petroleum Geoscience*, **14**, 3–15.
- Manzocchi, T., Heath, A.E., Palanathakumar, B., Childs, C. & Walsh, J.J. 2008b. Faults in conventional flow simulation models: a consideration of representational assumptions and geological uncertainties. *Petroleum Geoscience*, **14**, 91–110.
- Matthews, J.D., Carter, J.N., Stephen, K.D., Zimmerman, R.W., Skorstad, A., Manzocchi, T. & Howell, J.A. 2008. Assessing the effect of geological uncertainty on recovery estimates in shallow-marine reservoirs: the application of reservoir engineering to the SAIGUP project. *Petroleum Geoscience*, **14**, 35–44.
- Morrow, C.A., Sih, L.Q. & Byerlee, J.D. 1984. Permeability of fault gouge under confining pressure and shear stress. *Journal of Geophysical Research*, **89** (B5), 3139–3200.
- Ottesen Ellevset, S., Knipe, R.J., Olsen, T.S., Fisher, Q.T. & Jones, G. 1998. Fault controlled communication in the Sleipner Vest Field, Norwegian continental shelf: detailed quantitative input for reservoir simulation and well planning. In: Jones, G., Fisher, Q.J. & Knipe, R.J. (eds) *Faulting, Fault Sealing and Fluid Flow in Hydrocarbon Reservoirs*. Geological Society, London, Special Publications, **147**, 283–297.
- Pooler, J. & Amory, M. 1999. A subsurface perspective on ETAP – an integrated development of seven Central North Sea fields. In: Fleet, A.J. & Boldy, S.A.R. (eds) *Petroleum Geology of Northwest Europe: Proceedings of the 5th conference*. Geological Society, London, 993–1006.
- Robinson, P.C. 1983. Connectivity of fracture systems – a percolation theory approach. *Journal of Physics A: Mathematical and General*, **16**, 605–614.
- Schlishe, R.W., Young, S.S., Ackerman, R.V. & Gupta, A. 1996. Geometry and scaling relations of a population of very small rift-related normal faults. *Geology*, **24**, 683–686.
- Scholz, C.H. & Cowie, P.A. 1990. Determination of total strain from faulting using slip measurements. *Nature*, **346**, 837–839.
- Skorstad, A., Kolbjørnsen, O., Fjellvoll, B., Howell, J.A., Manzocchi, T. & Carter, J.N. 2005. Sensitivity of oil production to petrophysical heterogeneities. In: Leuangthong, O. & Deutsch, C. V. (eds) *Geostatistics Banff 2004. Quantitative Geology and Geostatistics*, **14**(2), 723–730.
- Skorstad, A., Kolbjørnsen, O., Manzocchi, T., Carter, J.N. & Howell, J.A. 2008. Combined effects of structural, stratigraphic and well controls on production variability in faulted shallow-marine reservoirs. *Petroleum Geoscience*, **14**, 45–54.
- Spaak, P., Almond, J., Salahudin, S., Mohd Salleh, Z. & Tosun, O. 1999. Fulmar: a mature field revisited. In: Fleet, A.J. & Boldy, S.A.R. (eds) *Petroleum Geology of Northwest Europe: Proceedings of the 5th conference*. Geological Society, London, 1089–1100.
- Sperrevik, S., Gillespie, P.A., Fisher, Q.J., Halvorsen, T. & Knipe, R.J. 2002. Empirical estimation of fault rock properties. In: Koestler, A.G. & Hunsdale, R. (eds) *Hydrocarbon Seal Quantification*. Norwegian Petroleum Society Special Publications, **11**, 109–125.
- Stephen, K.D., Yang, C., Carter, J.N., Howell, J.A., Manzocchi, T. & Skorstad, A. 2008. Upscaling uncertainty analysis in a shallow-marine environment. *Petroleum Geoscience*, **14**, 71–84.
- Stevens, V. 1991. The Beatrice Field, Block 11/30a, UK North Sea. In: Abbots, I.L. (ed.) *United Kingdom Oil and Gas Fields, 25 Years Commemorative Volume*. Geological Society, London, Memoirs, **14**, 245–252.
- Yielding, G., Freeman, B. & Needham, D.T. 1997. Quantitative fault seal prediction. *American Association of Petroleum Geologists Bulletin*, **81**, 897–917.
- Yielding, G., Overland, J.A. & Byberg, G. 1999. Characterization of fault zones in the Gullfaks Field for reservoir modelling. In: Fleet, A.J. & Boldy, S.A.R. (eds) *Petroleum Geology of Northwest Europe: Proceedings of the 5th conference*. Geological Society, London, 1177–1186.
- Yielding, G. 2002. Shale Gouge Ratio – calibration by geohistory. In: Koestler, A.G. & Hunsdale, R. (eds) *Hydrocarbon Seal Quantification*. Norwegian Petroleum Society Special Publications, **11**, 127–139.